Forced Rossby waves in a basin with a meridional barrier and bottom friction

J. ATHERTON
MIT/WHOI Joint Program in Physical Oceanography
Woods Hole Oceanographic Institution, Woods Hole, MA 02543, USA

(ricevuto il 10 Agosto 1999; approvato il 17 Gennaio 2000)

Summary. — The forced, linear, Rossby wave solution for a barotropic fluid in a square basin on a β plane containing a thin, continuous but pierced meridional barrier is examined. The forcing is zonally localized and vorticity is removed through bottom friction. The forcing is applied east of the barrier and is periodic in time. To the north and south of the barrier there are small gaps of equal width d separating the barrier from the basin walls. The value of the stream function on the walls of the basin is zero while the value of the stream function on the barrier, Ψ_I, is a function of time, the forcing structure and the forcing frequency. Ψ_I is determined by an application of Kelvin's theorem on a contour about the barrier and its value gives the flux between the two sub-basins that are formed by the barrier. The variance of the stream function is explored as a function of the forcing frequency for different meridional structures of the forcing. We investigate symmetric, antisymmetric, and asymmetric forcings about the mid-latitude of the basin. Peaks in the variance occur at frequencies where the solution is dominated by a full basin or sub-basin mode. It was found that modes which were antisymmetric about the mid-latitude could not propagate past the barrier, while modes which were symmetric about the mid-latitude always had some propagation past the barrier. For the case of eastern sub-basin modes which are symmetric about the mid-latitude this propagation is minute. The sensitivity of the solutions to bottom friction is also discussed. As friction is increased, the peaks in the variance become broader and begin to merge. At sufficiently high values of bottom friction a combination of modes, rather than one single mode, dominates the solution at a peak frequency.

PACS 92.10 – Physics of the oceans.
PACS 92.10.Fj – Dynamics of the upper ocean.
PACS 92.10.Ei – Coriolis effects.

1. – Introduction

The focus of this paper is to investigate how Rossby waves are able to propagate past a meridional barrier through narrow gaps which are much smaller than the meridional extent of the wave. The idea to investigate a Rossby wave propagating

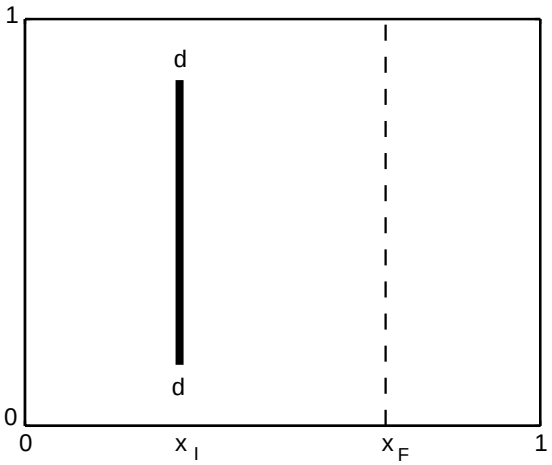

Fig. 1. – Sketch of the square basin with the meridional island placed at x_{I} and the forcing along the dotted line at x_{F}. There are two gaps of width d to the north and south of the barrier.

through such narrow gaps first occurred to Pedlosky and Spall (1999) when examining a simple two-layer baroclinic numerical model, the steady-flow problem examined by Pedlosky *et al.* (1997). They noticed that the boundary layer to the east of the barrier became unstable and developed eddies, at the same time it was apparent in the lower layer, which had a fairly weak mean flow, that, what seemed to be basin scale Rossby normal modes had developed. The normal mode, while existing in both layers, was masked by the mean flow and its instability in the upper layer. See the introduction and figures 1 (a) and (b) to Pedlosky and Spall (1999) for further details.

Naturally this observation lead them to ask how could it be possible to excite basin scale normal modes when the forcing was so isolated in the eastern sub-basin with only very narrow gaps opening to the western sub-basin. Their first step was to determine the nature of the Rossby normal modes by solving both analytically and numerically for the normal modes in a rectangular basin with a meridional island. By including a periodic forcing to the east of the barrier and bottom friction, this paper is an extension of their analytical work. In this manner we investigate the excitation of the normal modes, their amplitudes and the general issue of the propagation of wave energy through barriers containing narrow gaps. The basin shape used in this paper is shown in fig. 1. It is a square basin with a thin meridional barrier at x_{I}. There are two gaps of width d to the north and south of the barrier separating the barrier from the basin walls. The forcing is periodic and occupies the dotted line in fig. 1.

Section **2** of this paper is a description of the theory for the model and presents the analytical solution to the problem. Subsection **3**˙1 is a general discussion of the full basin and sub-basin modes, subsect. **3**˙2 investigates some of the larger modes where the meridional structure of the forcing is symmetric, antisymmetric and asymmetric about the mid-latitude. Finally subsect. **3**˙3 considers the effects of friction.

The model pertains to the oceanic flow around topographic features such as islands and ridges. Its most direct oceanographic application is in understanding the abyssal circulation as it encounters the mid-ocean ridge system and its many fracture zones.

The forcing can be thought of as that due to wind stress, Ekman pumping, or abyssal upwelling, depending on the situation being considered.

Compared to the real ocean, this study contains many simplifying assumptions, therefore our solutions will not directly mimic real oceanic circulations. However, the physics contained in this study occur in nature, and this simplified model should shed some light on the situation. It will also serve as a building block to the solutions of situations of greater complexity which should more closely resemble the motions observed in nature.

2. – Theory

The linear, quasi-geostrophic potential vorticity equation on the β plane for a barotropic fluid with forcing and bottom friction is (Pedlosky (1987))

$$\nabla^2 \Psi_t(x, y, t) + \beta \Psi_x(x, y, t) = F(x, y, t) - r\nabla^2 \Psi(x, y, t). \tag{1}$$

There is no vortex stretching term since the Rossby radius of deformation is assumed to be large in comparison to the horizontal length scale of the flow. This is equivalent to a rigid lid boundary condition.

The stream function is related to the pressure, P, by $\Psi = 1/(f_0 \varrho_0) P$, where f_0 is the reference value of the Coriolis parameter which is given by $f = f_0 + \beta y$ in the β plane approximation, and ϱ_0 is the constant density.

As previously mentioned, the forcing can be either a wind stress curl, Ekman pumping, or an upwelling from the abyss into the thermocline as in Stommel and Arons (1960). If the forcing is a wind stress curl the full Sverdrup transport is considered. If the forcing is an Ekman pumping only the geostrophic component of the transport is present. The model really can account for both situations since the quasi-geostrophic theory to first order ignores the mass flux in the Ekman layer.

The variables are non-dimensionalized as follows:

$$t = (\beta L)^{-1} t', \tag{2}$$

$$(x, y) = L(x', y'), \tag{3}$$

$$F(x, y, t) = F_0 T(x', y', t'), \tag{4}$$

$$\Psi(x, y, t) = \frac{F_0 L \Phi(x', y', t')}{\beta} \tag{5}$$

and the non-dimensionalized form of (1) is

$$\nabla^2 \Phi_t(x', y', t') + \Phi_x(x', y', t') = T(x', y', t') - \gamma \nabla^2 \Phi(x', y', t'), \tag{6}$$

where $\gamma = r/\beta L$ is the dimensionless friction parameter. All of the dimensionless variables (x', y', t') are of order one. From this point on, for clarity, the primes will be dropped.

A force that oscillates in time is used and the following substitutions are made:

$$\Phi(x, y, t) = e^{-i(\omega t + k(x - x_I))} \phi(x, y), \tag{7}$$

$$T(x, y, t) = e^{-i\omega t} T(x, y), \tag{8}$$

where $k = 1/(2(\omega + i\gamma))$ and x_I is the zonal position of the thin meridional barrier. This results in the inhomogeneous Helmholtz equation for $\phi(x, y)$

$$\nabla^2 \phi(x, y) + k^2 \phi(x, y) = \frac{i}{\Omega} e^{ik(x - x_I)} T(x, y), \tag{9}$$

where $\Omega = \omega + i\gamma$.

The forcing is assumed to be a delta-function in the zonal direction at $x = x_F$. The meridional structure of $T(x, y)$ and the complete structure of $\phi(x, y)$ are represented by a Fourier sine series in y as follows:

$$\phi(x, y) = \sum_{n=1}^{\infty} \phi_n(x) \sin(n\pi y), \tag{10}$$

$$T(x, y) = \delta(x - x_F) \sum_{n=1}^{\infty} T_n \sin(n\pi y). \tag{11}$$

The Fourier coefficients, $\phi_n(x)$, are functions of x to be determined. The boundary condition of no normal flow at $y = 0$ and $y = 1$ is now satisfied since $\phi(x, y)$ has been expressed as a Fourier sine series, and hence vanishes at $y = 0$ and $y = 1$.

The above substitutions for $\phi(x, y)$ and $T(x, y)$ lead to the following second-order ordinary differential equation in x for each Fourier coefficient $\phi_n(x)$:

$$\frac{d^2 \phi_n(x)}{dx^2} - \alpha_n^2 \phi_n(x) = \frac{i}{\Omega} e^{ik(x - x_I)} T_n \delta(x - x_F), \tag{12}$$

where $\alpha_n^2 = n^2 \pi^2 - k^2$. The solution to this equation in the basin interior involves solving the second-order homogeneous equation

$$\frac{d^2 \phi_n(x)}{dx^2} - \alpha_n^2 \phi_n(x) = 0 \tag{13}$$

in the three regions

$$\begin{aligned} 0 &< x < x_I, \\ x_I &< x < x_F, \\ x_F &< x < 1, \end{aligned}$$

leading to a total of six unknown constants. Therefore six boundary conditions are required to determine these constants. The condition of no normal flow at $x = 0$ and $x = 1$ requires the total stream function to be zero at the basin walls. Another two boundary conditions arise from matching the solution at the zonal position of the delta function of the forcing $x = x_F$. The stream function is continuous at this point and so provides the first of these, and integrating (12) from $x_F - \varepsilon$ to $x_F + \varepsilon$ and taking the limit as ε goes to zero yields the second matching condition for the first derivative of $\phi_n(x)$. The last two unknown coefficients are determined by assuming that the total

stream function has the form

$$\Phi(x_I, y, t) = e^{-i\omega t}\begin{cases} \frac{y}{d}\phi_I & \text{for} \quad 0 < y < d, \\ \phi_I & \text{for} \quad d < y < 1-d, \\ \frac{1-y}{d}\phi_I & \text{for} \quad 1-d < y < 1, \end{cases} \tag{14}$$

at $x = x_I$, where ϕ_I is a constant such that the full stream function on the barrier is $\Phi(x_I, t) = e^{-i\omega t}\phi_I$. A no normal flow condition at the barrier dictates that ϕ_I must be independent of y. It should be noted that ϕ_I is a function of the meridional structure of the forcing, the forcing frequency, and the friction parameter and must be determined as part of the solution. The form (14) holds for $d \ll 1$ and assumes the flow is zonal, independent of y and time periodic in the region of the narrow gaps. See Pedlosky and Spall (1999) for a comparison of this linear assumption to numerical results, without the presence of friction. The linear assumption is valid as long as the Stommel boundary layer is small compared to the gap width.

The assumed form for the stream function at $x = x_I$, see (14), is expanded in a Fourier sine series and its Fourier coefficient functions, $\phi_n(x_I)$, are matched to the solutions of (12) in the regions $0 < x < x_I$ and $x_I < x < x_F$ on the line $x = x_I$.

At this point the Fourier coefficients $\phi_n(x)$ are determined in terms of the forcing and ϕ_I. The solutions are

In the region $0 < x < x_I$

$$\phi_n(x) = E_n \sinh \alpha_n(x), \tag{15}$$

In the region $x_I < x < x_F$

$$\phi_n(x) = C_n \sinh \alpha_n(x - x_I) + D_n \cosh \alpha_n(x - x_I), \tag{16}$$

In the region $x_F < x < 1$

$$\phi_n(x) = A_n \sinh \alpha_n(x - 1) \tag{17}$$

with

$$D_n = \frac{4\phi_I \sin(n\pi d)\, M(n)}{n^2\pi^2 d}, \tag{18}$$

$$M(n) = \begin{cases} 0, & \text{if } n = \text{even}, \\ 1, & \text{if } n = \text{odd}, \end{cases} \tag{19}$$

$$C_n = \frac{1}{\alpha_n \sinh \alpha_n(1 - x_I)}\left(T_n \sinh \alpha_n(x_F - 1) - D_n \alpha_n \cosh \alpha_n(1 - x_I)\right), \tag{20}$$

$$A_n = \frac{1}{\sinh \alpha_n(x_F - 1)}\left(C_n \sinh \alpha_n(x_F - x_I) + D_n \cosh \alpha_n(x_F - x_I)\right), \tag{21}$$

$$E_n = \frac{D_n}{\sinh \alpha_n x_I}. \tag{22}$$

Finally, to determine the value of ϕ_I, the tangential component of the horizontal momentum equation

$$\frac{\partial \vec{u}}{\partial t} + (\zeta + f)\,\hat{k} \times \vec{u} = -\nabla\left(\frac{p}{\varrho} + \frac{|u|^2}{2}\right) - r\vec{u} \tag{23}$$

is integrated around the barrier.

The integral of the second term on the left side is equal to zero due to the boundary condition of no normal flow. The integral of the first term on the right side is also zero since it is the integral of a perfect differential. The two remaining terms lead to the following ordinary differential equation with respect to time for the circulation integral, which is Kelvin's theorem applied on a contour encircling the barrier:

$$\left(\frac{\partial}{\partial t} + r\right) \oint \vec{u} \cdot \mathrm{d}\vec{s} = 0\,. \tag{24}$$

The transient solutions decay exponentially in time leaving a periodic solution. Therefore, after the transients have decayed away, the "island" boundary condition is

$$\oint \vec{u} \cdot \mathrm{d}\vec{s} = 0\,. \tag{25}$$

Considering the geometry of the barrier the above integral becomes

$$\int_d^{1-d} v_+(x_I)\,\mathrm{d}y = \int_d^{1-d} v_-(x_I)\,\mathrm{d}y\,, \tag{26}$$

where $v_+(x_I) = \sum_{n=1}^{\infty} \frac{\partial \Phi_+}{\partial x}\Big|_{x=x_I} \sin(n\pi y)$ and $v_-(x_I) = \sum_{n=1}^{\infty} \frac{\partial \Phi_-}{\partial x}\Big|_{x=x_I} \sin(n\pi y)$. The negative subscript refers to the solution just west of the barrier, likewise the positive subscript refers to the solution just east of the barrier. After making the substitutions for the meridional velocities, a solution for the time-independent part of the stream function on the barrier is obtained:

$$\phi_I = \frac{\sum_{n=\mathrm{odd}}^{\infty} \frac{2F_n \sinh \alpha_n (x_F - 1)\cos(n\pi d)}{\pi n \sinh \alpha_n (1 - x_I)}}{\sum_{n=\mathrm{odd}}^{\infty} \frac{\alpha_n \sin(n\pi d)\cos(n\pi d)\sinh(\alpha_n)}{n^3\pi^3 d \sinh \alpha_n (1 - x_I)\sinh \alpha_n (x_I)}}\,. \tag{27}$$

For the even components the equation is trivially satisfied and provides no information about ϕ_I. Considering the solution in the western basin (15), we see that the Fourier coefficient functions are zero when n is even implying that there is no transport between the basin and the barrier for these modes. The conclusion is that even components, corresponding to motions which are antisymmetric about the mid-latitude $y = 0.5$, make no contribution to the value ϕ_I.

If the odd Fourier components of the forcing, T_n, are zero, it follows that $\phi_I = 0$. Therefore a forcing which is antisymmetric about $y = 0.5$ will yield no flow through the gaps, and from (15) it follows that there would then be no response in the western basin.

The variance of the response was calculated by integrating the absolute value of the stream function over the area of the basin

$$\text{variance} = \int_0^1 \int_0^1 \Phi\Phi^* \, \mathrm{d}x \, \mathrm{d}y \tag{28}$$

recalling that $\Phi(x, y, t) = e^{-i(\omega t + k(x - x_1))} \sum_{n=1}^{\infty} \phi_n(x) \sin(n\pi y)$. The final expression for the variance along with an expression for the integral of the meridional velocity v_+ on the eastern side of the barrier alone

$$\mathrm{EC} = \int_d^{1-d} v_+(x_\mathrm{I}) \, \mathrm{d}y \tag{29}$$

is shown in the appendix.

3. – Results and discussion

3·1. *General discussion of full-basin and sub-basin modes.* – Before proceeding with a description of the parameters, forcing, and subsequent results for this study, we would like to discuss some general features of the full basin and sub-basin modes appearing in the solution.

A full basin mode appears on both sides of the barrier, whereas a sub-basin mode only appears on one side of the barrier. We call them sub-basin modes because they are normal modes for the eastern and western sub-basins formed by the barrier which nearly divides the basin in two.

Unlike the normal modes for the basin in the absence of the barrier which correspond to a single Fourier component in y, Pedlosky (1987), the normal-modes for the basin containing the barrier are a combination of Fourier components. One way to see that this is the case is to recall that any solution of the problem must have the form (14) at the zonal position $x = x_\mathrm{I}$. At $x = x_\mathrm{I}$ our solution is a Fourier sine series of (14) which cannot be represented by a single Fourier component.

Considering this major difference between the two solutions it is surprising that many of the normal modes closely resemble one another, both in their natural frequencies and their spatial structure. It is this heuristic relationship that we wish to illustrate at this point.

We begin by noting that the coefficient C_n (20) which appears in the solution of the stream function to the east of the barrier contains the term $\sinh \alpha_n(1 - x_\mathrm{I})$, where $\alpha_n^2 = n^2\pi^2 - k^2$ and $k = \dfrac{1}{2(\omega + i\gamma)}$, in the denominator. Therefore the solution will become very large as $\sinh \alpha_n(1 - x_\mathrm{I})$ becomes very small. As long as friction is present $\sinh \alpha_n(1 - x_\mathrm{I})$ can never equal zero. If we allow ourselves for the purpose of illustration to eliminate the friction by setting $\gamma = 0$, we can solve for the values of ω for which $\sinh \alpha_n(1 - x_\mathrm{I})$ equals zero. The result is $\omega = \dfrac{1}{2\pi\sqrt{\left(n^2 + \dfrac{m^2}{(1 - x_\mathrm{I})^2}\right)}}$, where m and n are integers. These are the eigenfrequencies for the normal modes of a basin the size of the eastern sub-basin.

TABLE I. – *Comparison of the nine basin modes in this paper to the normal modes for a barrier free basin to which they resemble. The resemblance is observed both in the contour plots and in the frequencies. For the case of the sub-basin modes the barrier free basin has the same size as the sub-basin.*

Mode for basin with barrier	Mode for basin without barrier
1st Full Basin Mode $\omega = 0.1057$	$m = 1, n = 1$ $\omega = 0.1125$
2nd Full Basin Mode $\omega = 0.0686$	$m = 2, n = 1$ $\omega = 0.0712$
1st Eastern Sub-basin Mode $\omega = 0.0648$	$m = 1, n = 2$ $\omega = 0.0648$
3rd Full Basin Mode $\omega = 0.0503$	$m = 3, n = 1$ $\omega = 0.0503$
2nd Eastern Sub-basin Mode $\omega = 0.0479$	$m = 1, n = 3$ $\omega = 0.0479$
3rd Eastern Sub-basin Mode $\omega = 0.0456$	$m = 2, n = 2$ $\omega = 0.0456$
4th Full Basin Mode $\omega = 0.039$	
5th Full Basin Mode $\omega = 0.0381$	
1st Western Sub-basin Mode $\omega = 0.0356$	$m = 1, n = 3$ $\omega = 0.0356$

Likewise the coefficient E_n (22) appearing in the solution to the west of the barrier is seen to contain $\sinh \alpha_n(x_I)$ in its denominator. Again setting $\gamma = 0$ and solving for ω when $\sinh \alpha_n(x_I)$ equals zero we find $\omega = \dfrac{1}{2\pi\sqrt{\left(n^2 + \dfrac{m^2}{(x_I)^2}\right)}}$, where m and n are integers. These are the eigenfrequencies for a basin the size of our western sub-basin.

From the observations above we expect that the natural frequencies for the sub-basin modes should equal the eigenfrequencies for basins the size of the sub-basins when the friction parameter is small. This is indeed the case as shown in table I. Figures 7 (c), (e), (f), and (i) are the contour plots of the absolute value of the membrane functions, ϕ, for the sub-basin modes in table I. There is a remarkable resemblance between these contour plots and the contour plots of the normal modes whose eigenfrequencies are equal to the natural frequencies of these sub-basin modes.

There is also an empirical relationship between the full basin modes for the basin with a barrier and the normal modes of a basin without a barrier of the same size. The dispersion relation for the full basin modes correspond to a resonance of Φ_I and hence a zero of the denominator of (26). Even when the friction is very small, the natural frequencies of the basin containing the barrier are close but not equal to the eigenfrequencies of the barrier free basin, see table I. Again there is also a strong resemblance in their spatial structure, see figs. 7(a), (b), and (d). However there exist

modes for the basin with a barrier that do not resemble any modes of the barrier free basin. For example, see the 4th and 5th full basin modes in figs. 7(g), and (h).

These general observations between the normal modes for the basin containing a barrier and the normal modes for barrier free basins were first noticed by Pedlosky and Spall (1999).

3·2. *Investigation of individual modes.* – The non-dimensional value of the friction parameter was taken to be very small, $\gamma = 10^{-8}$, so that individual modes could easily dominate the solution when the forcing occurred at their natural frequency. The cases of symmetric, antisymmetric, and asymmetric forcing about the mid-latitude, $y = 0.5$, are considered. To avoid placing the barrier at a position where the two sub-basins and the full basin could all have the same natural frequency, *i.e.* ensuring that the ratio of zonal extents of the sub-basins is not a ratio of integers, we arbitrarily put the barrier at $x_I = 0.3$. The forcing is arbitrarily put at $x_F = 0.7$.

For each case the variance for the full basin, western sub-basin, eastern sub-basin, and $|\phi_I|$ are plotted as a function of the forcing frequency. See figs. 2(a), (b), and (c), 4(a), and (b), and 6(a), (b), and (c). Since γ is small, the peaks in the variance are well defined and will correspond to forcing frequencies that are very close to the natural frequencies of the basin.

As mentioned before, due to the assumption that the stream function is linear in y in the gap, the gap width must remain small compared to the length scale of the problem. Changing the gap width results only in very slight changes in the natural frequencies of the full basin modes and hardly any changes in their contour plots. Therefore, the gap width is set at $d = 0.05$ and is kept at that value.

As noted in sect. **2**, the forcing has the form of a delta-function in x at x_F times a Fourier sine series in y (11). The symmetric, antisymmetric and asymmetric cases about the mid-latitude, $y = 0.5$, that will be considered are constructed from approximate delta-functions in y. The n-th Fourier coefficient in a sine series representing a delta-function at y_0 is given by

$$T_n = 2 \sin(n\pi y_0). \tag{30}$$

In the following cases the Fourier coefficients used will be

$$T_n = 2 \sin(n\pi y_0)\, e^{-(1/10)n^2}. \tag{31}$$

The factor $e^{-(1/10)n^2}$ gives more emphasis to the lower index terms, so this approximate delta-function will be spread out in the meridional direction about y_0. Two advantages result from defining the Fourier coefficients in this way. First, there is a smaller error involved in using a finite sum for the Fourier series since the higher-order terms are smaller leading to more rapid convergence (the first 50 terms are used in this paper). Second, the meridional structure of the modes will always have a scale much greater than the gap width where we have approximated our solution.

3·2.1. Symmetric forcing about the mid-latitude. The symmetric forcing was represented by a delta-function in x at $x_F = 0.7$ and an approximate delta-function in y at $y = 0.5$. The Fourier coefficients of the forcing were defined as in (31) with $y_0 = 0.5$.

Figures 2(a), (b), and (c) are semilog plots of the variance for the full basin, variance for the western sub-basin and variance for the eastern sub basin, respectively.

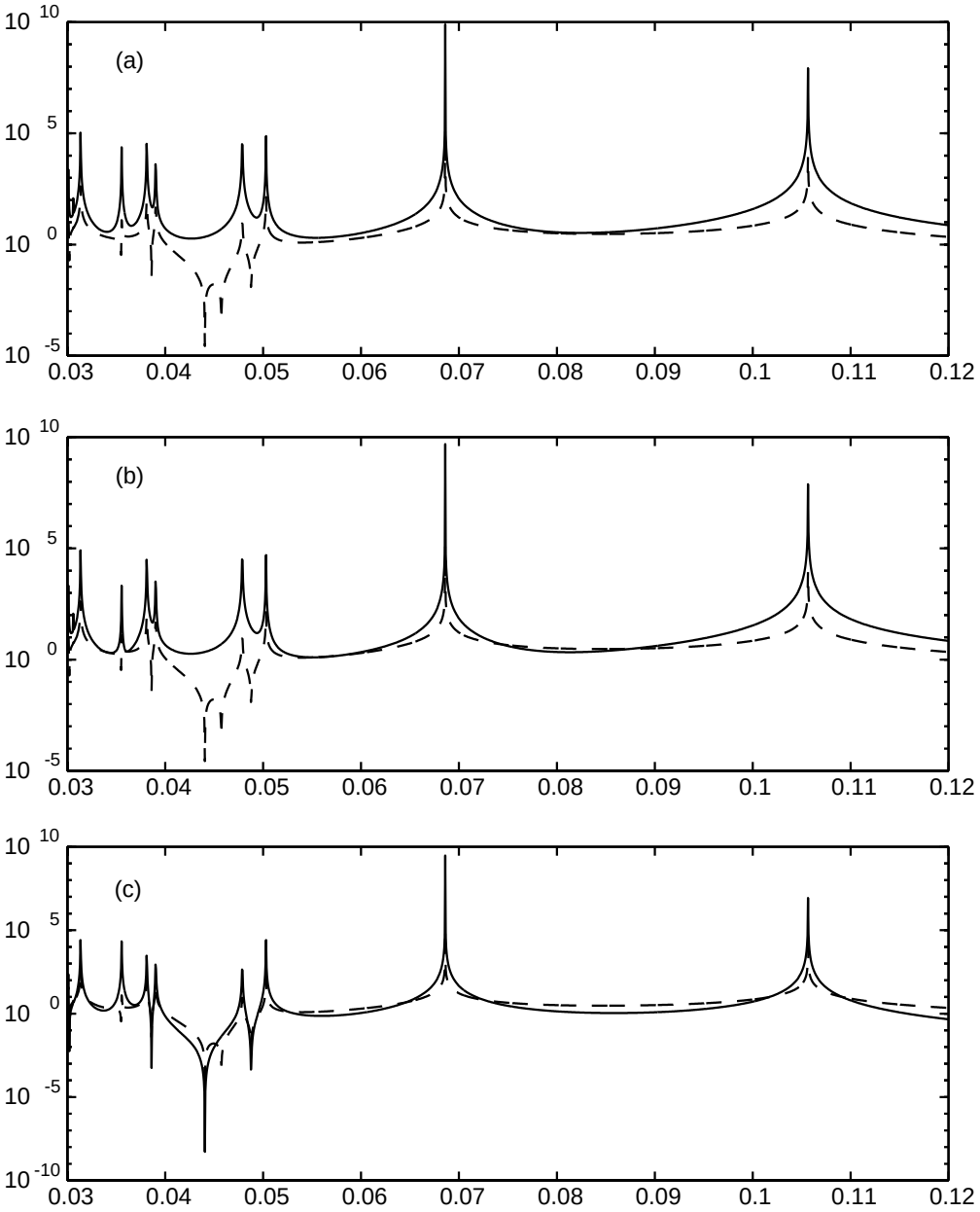

Fig. 2. – Semilog plots of $|\phi_{\mathrm{I}}|$ (- - -) and (a) full basin variance, (b) eastern sub-basin variance and (c) western sub-basin variance *vs.* forcing frequency ω for the case where $x_{\mathrm{I}} = 0.3$, $x_{\mathrm{F}} = 0.7$, $d = 0.05$, $\gamma = 10^{-8}$ and the meridional structure of the forcing is symmetric about $y = 0.5$. Note that the peak in $|\phi_{\mathrm{I}}|$ at $\omega = 0.0449$ is a minimum of ϕ_{I}.

Henceforth these will be referred to as the full variance, western variance, and eastern variance. Figures 3(a) to (g) are contour plots of the absolute value of the envelope of

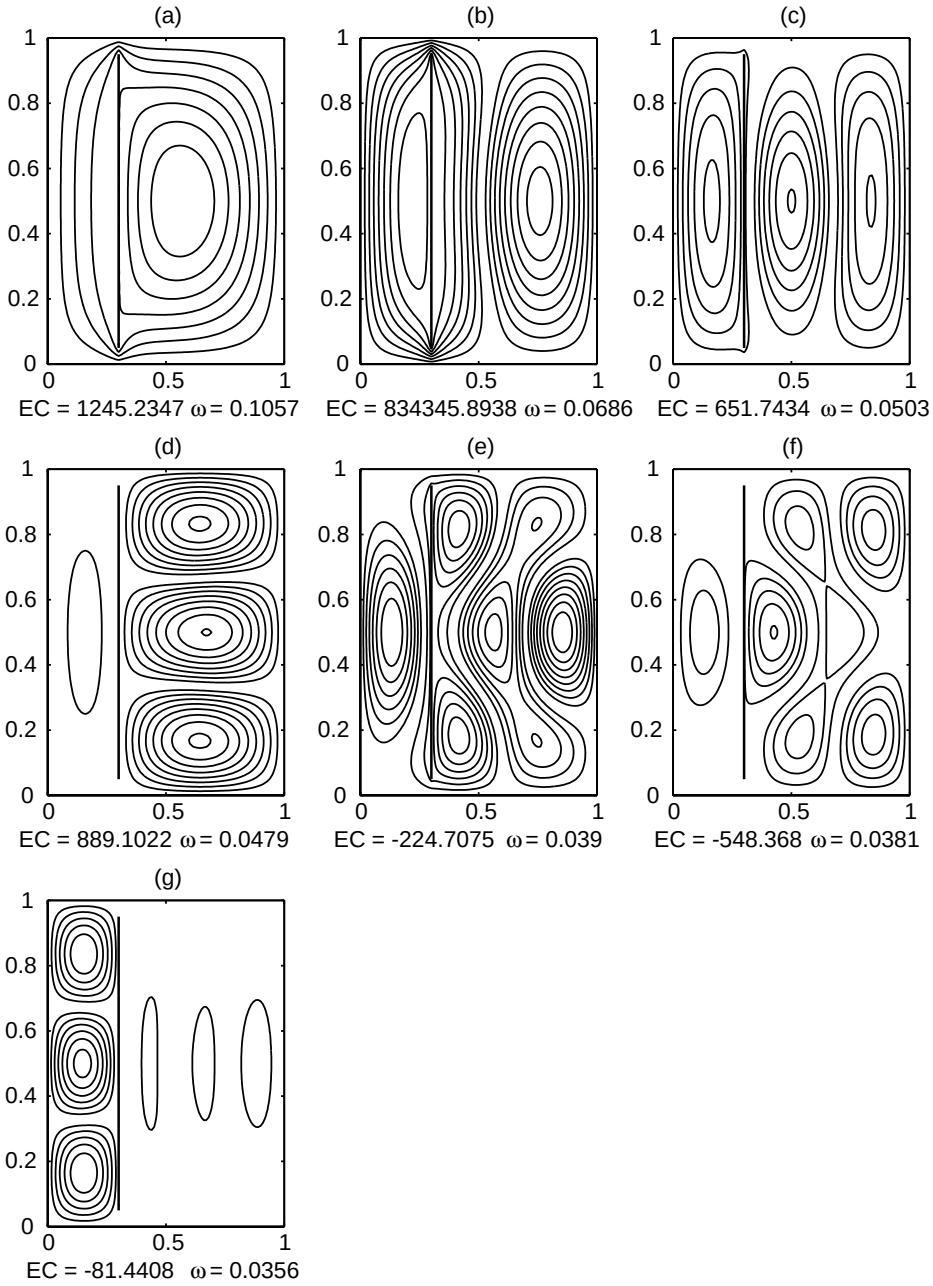

Fig. 3. – Contour plots for the case where $x_I = 0.3$, $x_F = 0.7$, $d = 0.05$, $\gamma = 10^{-8}$, and the meridional structure of the forcing is symmetric about $y = 0.5$. The forcing frequencies, shown on the plots, correspond to the first 7 peaks in the full basin variance graph in fig. 2(a). The value EC shown next to the forcing frequency is the circulation on the eastern side of the barrier (see appendix).

the stream function, *i.e.* $|\phi|$. The contour plots in fig. 3 were plotted with forcing frequencies corresponding to the first seven peaks in the full variance plot in fig. 2(a). The reason for stopping at the 7th peak is because this is the first western sub-basin mode to appear, see table I. Therefore these 7 peaks allow us to examine 5 full basin modes (fig. 3(a), (b), (c), (e), and (f)), one eastern sub-basin mode (fig. 3(d)) and one western sub-basin mode (fig. 3(g)). Starting from the right in fig. 2(a) the full basin modes occur at peaks 1, 2, 3, 5, and 6, the eastern sub-basin mode occurs at peak 4, and the western sub-basin mode occurs at peak 7, that is the peaks are numbered in order of decreasing frequency.

In this paper when we say that a mode occurs at a certain frequency, we mean that the mode dominates the solution at that frequency. The mode will dominate the solution because the forcing frequency is close to the mode's natural frequency and the friction, being relatively small, allows resonance to occur. This resonance allows us to easily find the normal modes.

Inspection of the contour plots in fig. 3 shows that there are no modes appearing that are antisymmetric about $y = 0.5$. One would not expect to see antisymmetric modes about $y = 0.5$, which correspond to even Fourier components, since the forcing used was symmetric about $y = 0.5$, and therefore only had odd nonzero Fourier components.

Considering the contour plots of the full basin modes in fig. 3(a), (b), (c), (e), and (f) and the semilog plots of the variances and $|\phi_{\mathrm{I}}|$ in fig. 2(a), (b), and (c), it is seen that these full basin modes peak in the full variance, western variance, eastern variance, and $|\phi_{\mathrm{I}}|$. Since there is a strong flow over the total area of the basin associated with each of these full basin modes, it is not surprising that these modes peak in all of the plots and coincide. When considering the contour plot in fig. 3(d) which clearly has a dominant flow in the eastern sub-basin and shows a strong resemblance to the normal mode ($m = 3$, $n = 1$) for a basin with no barrier and of the size of the eastern sub-basin, we were surprised to see that there was also a weak flow in the western sub-basin, and that this flow had a corresponding peak in the western variance and $|\phi_{\mathrm{I}}|$ (fig. 2(b)) although with much smaller magnitude than the peaks in the full variance and the eastern variance (fig. 2(a) and (c)). The explanation for this unexpected behavior lies in the fact that the circulation on the eastern side of the barrier is not zero (see EC in the caption of fig. 3(d)). The flow in the western sub-basin is necessary to satisfy the "island" boundary condition that the total circulation about the barrier is zero. Therefore it is the combined resonance in the eastern sub-basin and the need to satisfy a no net circulation condition around the barrier that causes the peak in the western variance and $|\phi_{\mathrm{I}}|$.

Considering the expressions for ϕ_{I}, (27), $\phi(x, y)$, (10), (15) and (22) in the western sub-basin, and the circulation to the east of the barrier EC (35) (see appendix), one sees that only the odd Fourier components contribute. Therefore one could predict that whenever the forcing is symmetric or asymmetric and contains odd Fourier components the above expressions will be nonzero. This follows as the linear independence of the individual terms of the Fourier series implies that their summation equals zero if and only if all of their Fourier coefficients are zero.

The same situation occurs when the western sub-basin mode in fig. 3(g) is considered. Surprisingly, although small in magnitude, there is a corresponding peak in the eastern variance at the frequency of this mode. Again, there is a significant circulation to the eastern side of the barrier which must be necessary to compensate for the fact that this western sub-basin mode cannot satisfy the "island" boundary

condition on its own. In this case, the circulation to the east of the barrier is transmitting very efficiently the forcing to the western sub-basin.

By consideration of the geometry of these modes which are symmetric about the mid-latitude, $y = 0.5$, it is seen that they will never be able to completely satisfy the circulation condition on one side of the barrier alone. Taking the mode $n = 3$ as an example, the two end cells next to the barrier have the same circulation, and the middle one has an opposite circulation. Therefore the circulation of the middle cell will never be able to fully cancel the circulation of the outer cells, except possibly if the barrier had the length 0.75. This situation cannot be treated with our approximation (14) which requires $d/L \ll 1$ since the gap width would be far too big. Therefore, for modes which are symmetric about the mid-latitude one should expect to see a small corresponding peak in the western variance for a eastern sub-basin mode and a corresponding peak in the eastern variance for a western sub-basin mode.

3·2.2. Antisymmetric forcing about the mid-latitude. Figures 4(a) and (b) show the full and eastern variances for the case where the y structure of the forcing is an approximate delta-function at $y = 0.75$ plus an approximate negative delta-function at $y = 0.25$. The Fourier coefficients for these delta-functions are defined as in (30) with $y_0 = 0.75$ and $y_0 = 0.25$. The western variance and ϕ_{I} are both zero for all forcing frequencies. For the purpose of comparison with the case of the symmetric forcing about the mid-latitude, only the first two peaks corresponding to frequencies greater than $\omega = 0.0356$ are considered. The contour plots of the absolute value of the envelope part of the stream function forced at these two peak frequencies are shown in fig. 4(c), and (d).

As a result of the antisymmetric forcing about the mid-latitude, the only modes that appear are also antisymmetric about the mid-latitude.

Since the full and eastern variances are identical and the western variance and ϕ_{I} are equal to zero, it follows that the only modes occurring are eastern sub-basin modes.

The explanation for this lies in the "island" circulation condition. Unlike the modes which are symmetric about the mid-latitude, these modes are able to completely satisfy the condition (25) since they contribute nothing to the circulation on the eastern side of the barrier. This is seen in fig. 4(c), and (d), where the EC is essentially zero (to within the computational error of the computer). By looking at equation (35) in appendix A we see that for antisymmetric modes which only have even Fourier components, EC is exactly equal to zero.

Turning again to the expressions for ϕ_{I}, (27), $\phi(x, y)$, (10), (15) and (22) in the western sub-basin, and the circulation to the east of the barrier EC (35) (see appendix), one sees that the even Fourier components never contribute to these parts of the solution. Therefore, if there are no odd Fourier components present, these components of the solution will always be zero. The circulation contribution of the eastern side of the barrier being zero implies that there is no need for movement on the western side of the barrier. The condition that the transport between the barrier and the basin, which is equivalent to ϕ_{I}, is zero means that the western sub-basin never "feels" the forcing and therefore will not have any circulation. Thus, with antisymmetric forcing about the mid-latitude there is never any movement in the western sub-basin, and hence full basin and western sub-basin modes do not appear.

An excellent comparison of a mode which is symmetric about the mid-latitude and can propagate past the barrier and a mode which is antisymmetric about the mid-latitude and cannot propagate past the barrier is shown in fig. 5(a) and (b). These

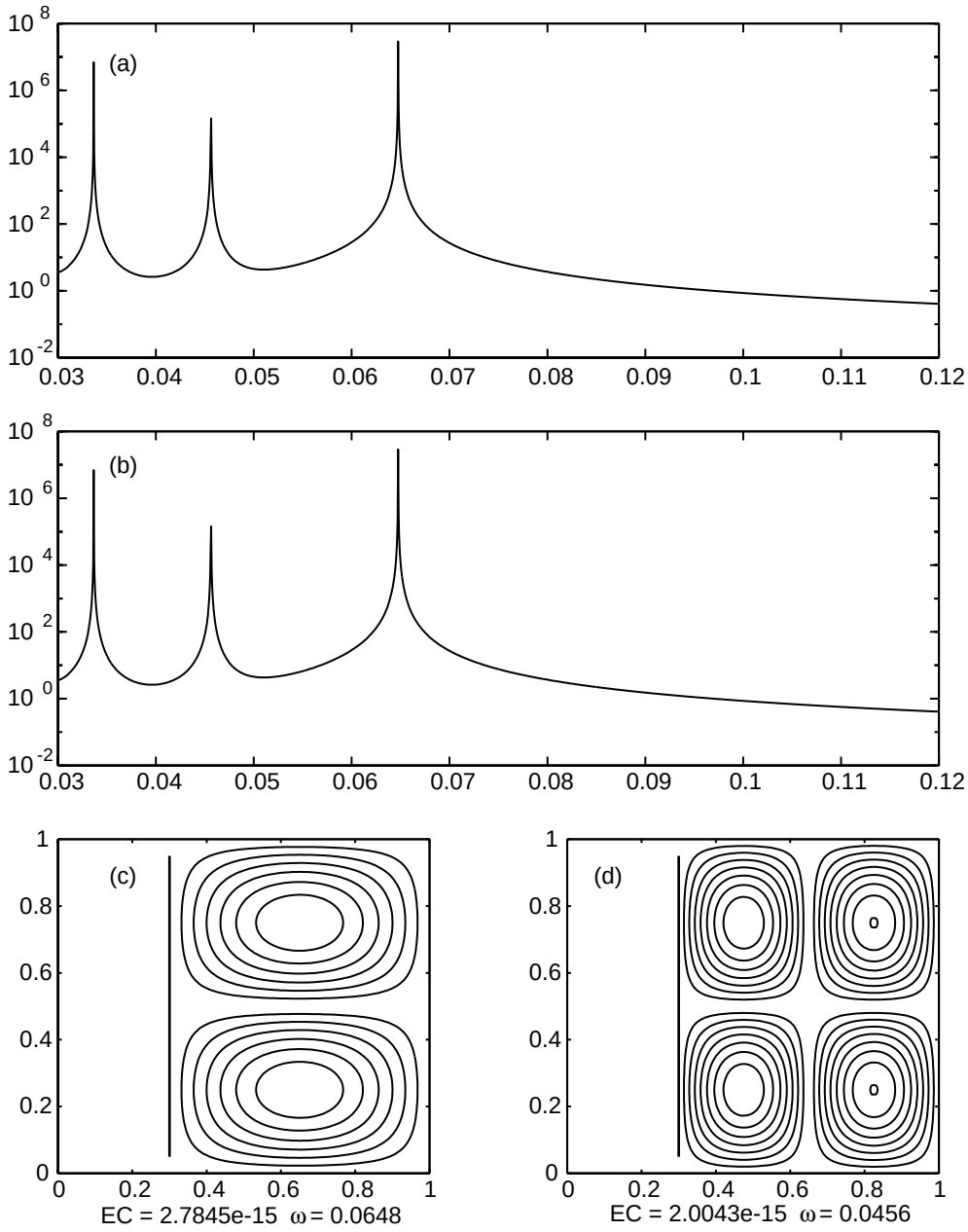

Fig. 4. – Semilog plots of (a) full basin variance, (b) eastern sub-basin variance *vs.* forcing frequency ω. Plots (c) and (d) are contours of $|\phi|$ at frequencies corresponding to the first two peaks of the full variance. This case is where $x_I = 0.3$, $x_F = 0.7$, $d = 0.05$, $\gamma = 10^{-8}$ and the meridional structure of the forcing is antisymmetric about $y = 0.5$.

figures both have the forcing at $x_F = 0.7$, the barrier at $x_I = 0.5$, a gap width of $d = 0.05$ and a friction parameter of $\gamma = 10^{-8}$.

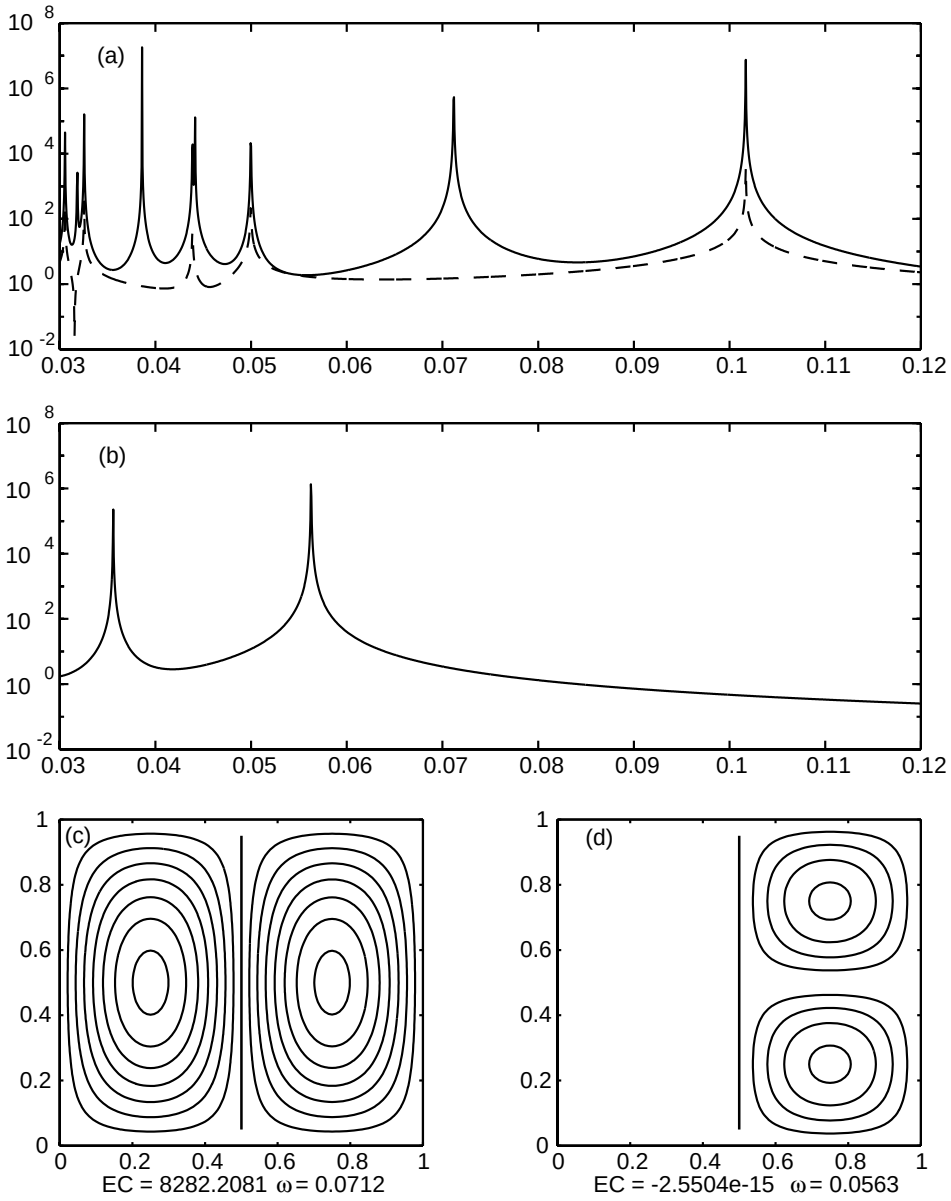

Fig. 5. – Semilog plots of the full variance and the contour plots for the case where $x_I = 0.5$, $x_F = 0.7$, $d = 0.05$, $\gamma = 10^{-8}$, and the meridional structure of the forcing is (a) and (c) symmetric about $y = 0.5$ and (b) and (d) antisymmetric about $y = 0.5$. The forcing frequencies, shown on the plots, correspond to (c) the natural frequencies of the western and eastern sub-basin modes resembling the ($m = 1$, $n = 1$) normal mode for a basin of the same size and the full basin mode resembling the normal mode ($m = 2$, $n = 1$) for a square basin the same size and no barrier and (d) the natural frequencies of the western and eastern sub-basin modes resembling the ($m = 1$, $n = 2$) normal mode for a basin of the same size and the full basin mode resembling the normal mode ($m = 2$, $n = 2$) for a square basin the same size and no barrier. The value EC shown next to the forcing frequency is the circulation on the eastern side of the barrier (see appendix).

Figure 5(a) is forced using the approximate delta-function at $y = 0.5$ and a frequency of $\omega = 0.0712$, which is the eigenfrequency for the normal mode ($m = 1$, $n = 1$) for a basin the size of the eastern and western sub-basins, and for the normal mode ($m = 2$, $n = 1$) for a basin the size of the full basin. For this full basin mode, the barrier position at $x_I = 0.5$ is exactly where the stream function is zero. Therefore, the barrier does not seem to have much effect on the flow and the natural frequency is equal to the eigenfrequency of the mode ($m = 2$, $n = 1$) for the basin in the absence of the barrier. We now have a special situation where the forcing frequency is at the resonant frequency of three different modes at the same time. For reasons already discussed, all three modes appear due to the symmetric meridional structure of the modes.

Figure 5(b) is constructed in the same way. The forcing is the approximate delta-function at $y = 0.75$ plus the negative approximate delta-function at $y = 0.25$. Also the forcing frequency is $\omega = 0.0563$ which is equal to the natural frequencies of the western and eastern sub-basins for the sub-basin modes resembling the normal mode ($m = 1$, $n = 2$) for a basin the size of the sub-basins and is equal to the natural frequency of the full basin mode resembling the normal mode ($m = 2$, $n = 2$) for a basin of corresponding size and no barrier. However this time, even though the forcing is at a natural frequency for three modes, the western sub-basin and full basin modes do not appear due to the fact that these modes are antisymmetric about the mid-latitude.

3·2.3. Asymmetric forcing about the mid-latitude. Figures 6(a), (b), and (c) show the full variance, western variance, and eastern variance for the case where the forcing is an approximate delta-function at $y = 0.75$. The forcing Fourier coefficients have been calculated as in (30) with $y_0 = 0.75$.

For this asymmetric forcing about the mid-latitude, odd and even Fourier components are present. The first 9 peaks in the full variance include the 7 peaks considered in the case of symmetric forcing about $y = 0.5$, and the 2 peaks considered in the case of antisymmetric forcing about $y = 0.5$.

The contour plots of the absolute value of $\phi(x, y)$ (10), corresponding to forcing frequencies equal to the frequencies of the peaks in the full variance, are shown in fig. 7(a) to (i). The contour plots of the different modes dominating the solution are the same as in the previous two forcing cases, except that a slight asymmetry due to the forcing is apparent in some of them. Figures 7(f) and (i) are examples where this asymmetry is particularly noticeable.

For all the modes which are symmetric about the mid-latitude (see fig. 7(a), (b), (d), (e), (g), (h), and (i)) EC is smaller in magnitude than it was when the forcing was symmetric. The modes which are antisymmetric about the mid-latitude (see fig. 7(c) and (f)) have a circulation to the east of the barrier greater than zero. Now that the forcing is asymmetric, one of the circulation cells is stronger than the other and there will not be exact cancellation as before. As mentioned above, the normal modes for the basin containing a barrier are made up of a spectrum of Fourier components. Now that the forcing is asymmetric there are both even and odd Fourier components present in the antisymmetric modes. It is the presence of the odd Fourier components which increases the circulation on the east side of the barrier. This can be seen in eq. (35) in the appendix.

3·3. *The effects of friction.* – Figures 8(a)-(f) show the variance for the case of asymmetric forcing where γ is increased. As γ is increased, the peaks become wider and eventually merge with their neighbors. Of course, the amplitude also decreases

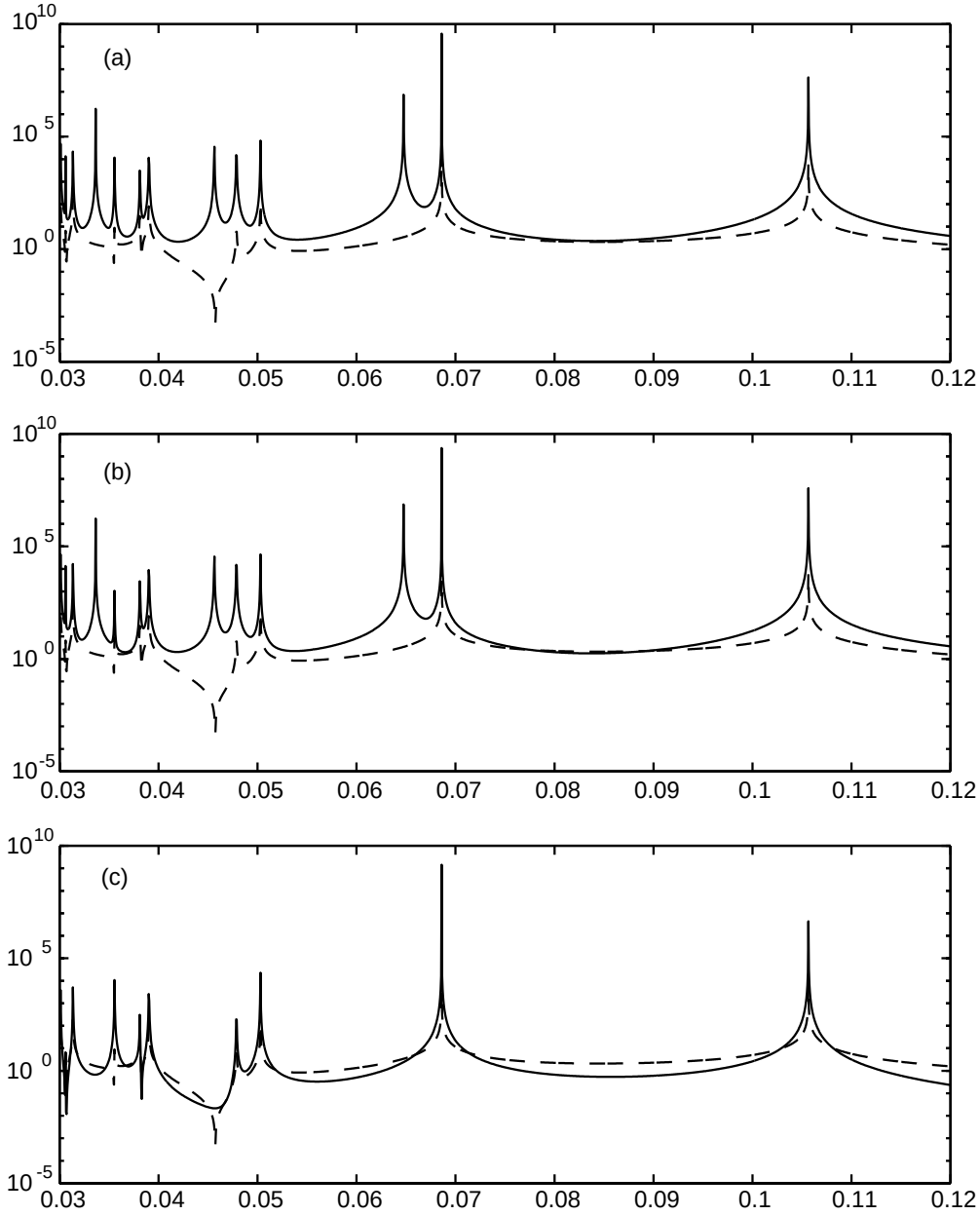

Fig. 6. – Semilog plots of $|\phi_I|$ (- - -) and (a) full basin variance, (b) eastern sub-basin variance and (c) western sub-basin variance *vs.* forcing frequency ω for the case where $x_I = 0.3$, $x_F = 0.7$, $d = 0.05$, $\gamma = 10^{-8}$, and the meridional structure of the forcing is asymmetric. Note that the peak in $|\phi_I|$ at $\omega = 0.0449$ is a minimum of ϕ_I.

significantly. Figure 8(f) uses a friction parameter of $\gamma = 0.0167$ which corresponds to a Stommel boundary layer, $\delta_s = r/\beta$, of 50 km and a basin length scale of 3000 km. Were

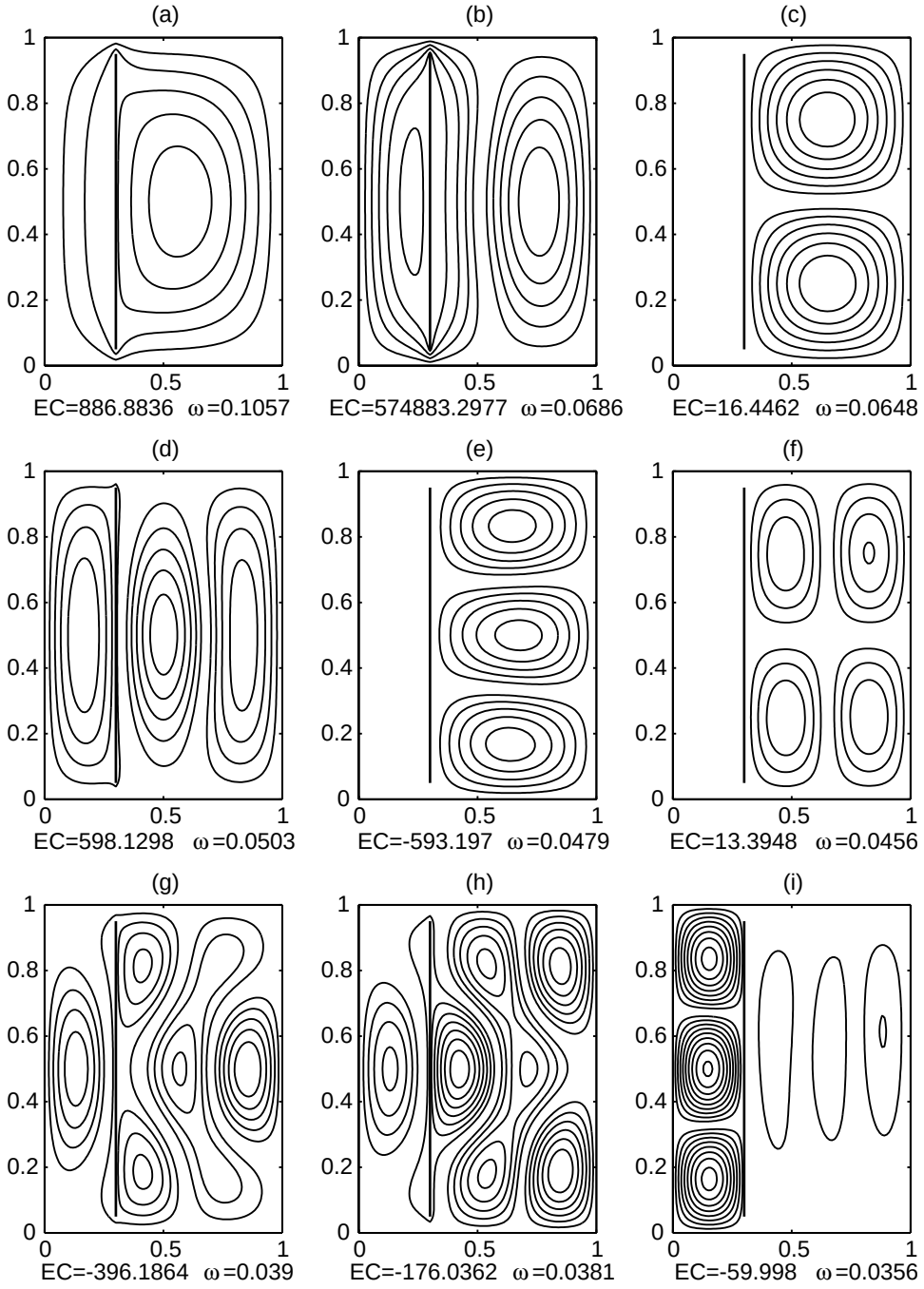

Fig. 7. – Contour plots for the case where $x_I = 0.3$, $x_F = 0.7$, $d = 0.05$, $\gamma = 10^{-8}$, and the meridional structure of the forcing is asymmetric. The forcing frequencies, shown on the plots, correspond to the first nine peaks in the full basin variance graph in fig. 5(a). The value EC shown next to the forcing frequency is the circulation on the east side of the barrier (see appendix).

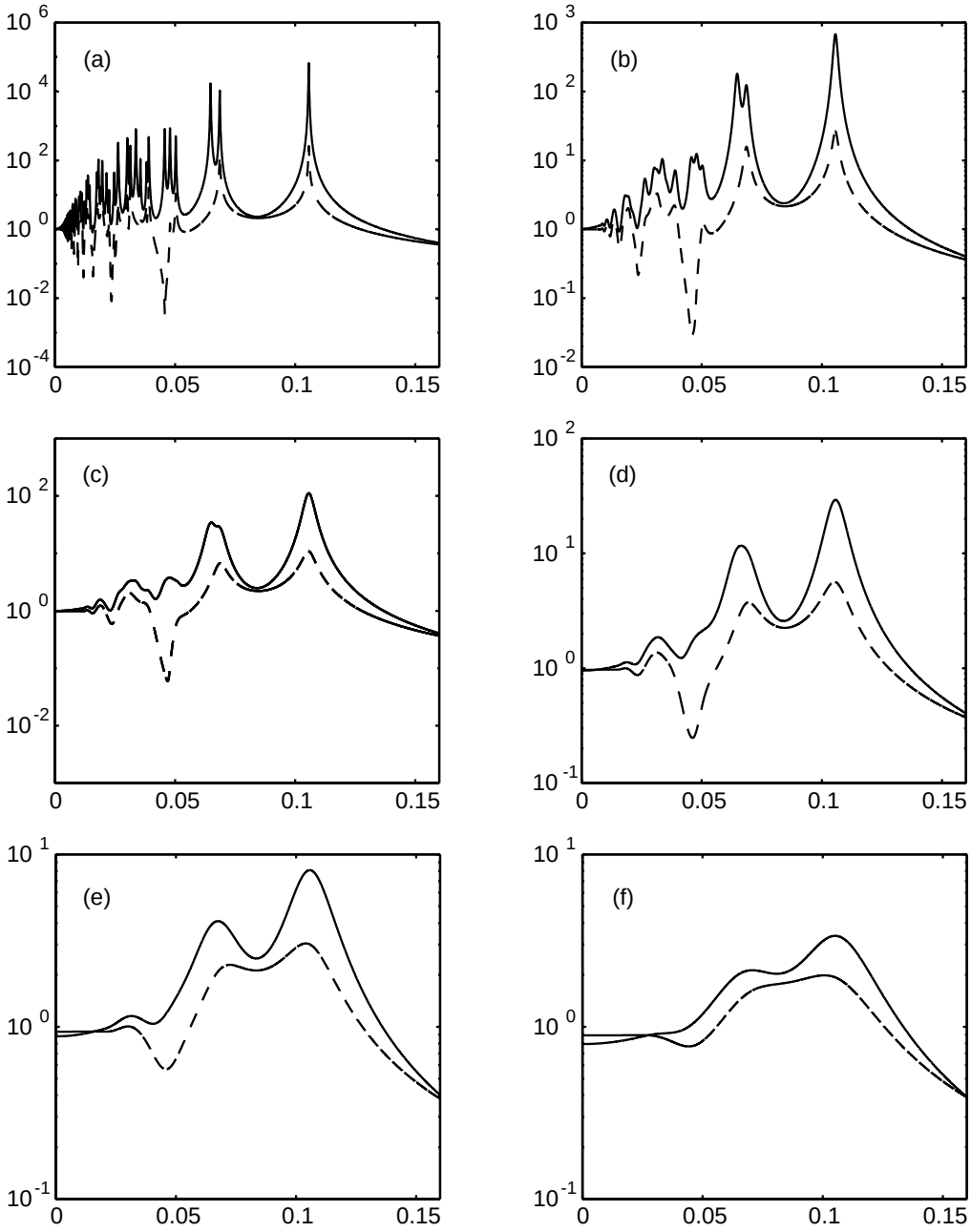

Fig. 8. – Semilog plots of $|\phi_{\mathrm{I}}|$ (---) and full basin variance *vs.* forcing frequency ω for the cases where $x_{\mathrm{I}} = 0.3$, $x_{\mathrm{F}} = 0.7$, $d = 0.05$, the meridional structure of the forcing is asymmetric, and varying friction (a) $\gamma = 0.0001$, (b) $\gamma = 0.001$, (c) $\gamma = 0.0025$, (d) $\gamma = 0.005$, (e) $\gamma = 0.01$, (f) $\gamma = 0.0167$.

the steady western boundary layer due to bottom friction, this would be the appropriate value for r to use. This is probably an overestimate for r since the actual western boundary current is inertial, so that r must be smaller than this derived value, suggesting that the peaks evident in figs. 8(c) and (f) are possibly plausible for real ocean basins absent complicating effects of nonlinearity and rough bottom topography.

4. – Summary and conclusions

The propagation of Rossby waves past a meridional barrier has been examined in detail by considering the different modes that dominate the solution when the basin is forced at or near their natural frequency with small bottom friction.

For a Rossby wave to propagate past the barrier, it is found that the forcing has to be either symmetric or asymmetric about the mid-latitude of the basin. This is because the only full basin and western sub-basin modes which occur are symmetric about the mid-latitude, and these modes will never be forced by a forcing which is antisymmetric about the mid-latitude. Even the eastern sub-basin modes which are symmetric about the mid-latitude have some propagation into the western sub-basin. This movement in the western sub-basin is caused by the requirement obtained from Kelvin's theorem, and it manifests itself as a peak in the western variance. Of course if the geometry is not symmetric, *e.g.* if the gaps are not symmetrically placed or the barrier is inclined to a longitude line, then these symmetry properties will be modified.

As friction is increased the modes merge together and, as seen in the previous section, it becomes increasingly difficult to determine which modes are present.

* * *

Thanks are due to my advisor J. Pedlosky for introducing me to this problem and for many helpful suggestions. This work was supported in part by National Science Foundation Grant No. OCE 93-0184 (F).

APPENDIX

Variance for full basin, eastern sub-basin and western sub-basin

The following are the full expressions for the variance for the full basin, the variance for the western sub-basin, and the variance for the eastern sub-basin, where a is the real part of α_n, b is the imaginary part of α_n, and $c = \gamma/(\omega^2 + \gamma^2)$.

(32) Full variance =

$$= \frac{e^{cx_I}}{2} \sum_{n=1}^{\infty} \left\{ \frac{|E_n|^2}{4} \left[e^{-cx_I} \left(\frac{e^{2ax_I}}{2a-c} + \frac{e^{-2ax_I}}{-2a-c} - \frac{e^{2ibx_I}}{2ib-c} - \frac{e^{-2ibx_I}}{-2ib-c} \right) - \right. \right.$$

$$\left. \left. - \left(\frac{1}{2a-c} + \frac{1}{-2a-c} - \frac{1}{2ib-c} - \frac{1}{-2ib-c} \right) \right] +$$

$$+\frac{|C_n|^2}{4}\left[e^{-cx_F}\left(\frac{e^{-2a(x_I-x_F)}}{2a-c}+\frac{e^{2a(x_I-x_F)}}{-2a-c}-\frac{e^{-2ib(x_I-x_F)}}{2ib-c}-\frac{e^{2ib(x_I-x_F)}}{-2ib-c}\right)-\right.$$

$$\left.-e^{-cx_I}\left(\frac{1}{2a-c}+\frac{1}{-2a-c}-\frac{1}{2ib-c}-\frac{1}{-2ib-c}\right)\right]+$$

$$+\frac{C_n^* D_n}{4}\left[e^{-cx_F}\left(\frac{e^{-2a(x_I-x_F)}}{2a-c}+\frac{e^{2a(x_I-x_F)}}{-2a-c}-\frac{e^{2ib(x_I-x_F)}}{-2ib-c}-\frac{e^{-2ib(x_I-x_F)}}{2ib-c}\right)-\right.$$

$$\left.-e^{-cx_I}\left(\frac{1}{2a-c}+\frac{1}{-2a-c}+\frac{1}{-2ib-c}-\frac{1}{2ib-c}\right)\right]+$$

$$+\frac{C_n D_n^*}{4}\left[e^{-cx_F}\left(\frac{e^{-2a(x_I-x_F)}}{2a-c}+\frac{e^{2a(x_I-x_F)}}{-2a-c}-\frac{e^{-2ib(x_I-x_F)}}{2ib-c}-\frac{e^{2ib(x_I-x_F)}}{-2ib-c}\right)-\right.$$

$$\left.-e^{-cx_I}\left(\frac{1}{2a-c}+\frac{1}{-2a-c}+\frac{1}{2ib-c}-\frac{1}{-2ib-c}\right)\right]+$$

$$+\frac{|D_n|^2}{4}\left[e^{-cx_F}\left(\frac{e^{-2a(x_I-x_F)}}{2a-c}+\frac{e^{2a(x_I-x_F)}}{-2a-c}+\frac{e^{2ib(x_I-x_F)}}{-2ib-c}+\frac{e^{-2ib(x_I-x_F)}}{2ib-c}\right)-\right.$$

$$\left.-e^{-cx_I}\left(\frac{1}{2a-c}+\frac{1}{-2a-c}+\frac{1}{-2ib-c}-\frac{1}{2ib-c}\right)\right]+$$

$$+\frac{|B_n|^2}{4}\left[-e^{-cx_F}\left(\frac{e^{2a(x_F-1)}}{2a-c}+\frac{e^{-2a(x_F-1)}}{-2a-c}-\frac{e^{2ib(x_F-1)}}{2ib-c}-\frac{e^{-2ib(x_F-1)}}{-2ib-c}\right)+\right.$$

$$\left.\left.+e^{-c}\left(\frac{1}{2a-c}+\frac{1}{-2a-c}-\frac{1}{2ib-c}-\frac{1}{-2ib-c}\right)\right]\right\}.$$

(33) Western variance =

$$=\frac{e^{cx_I}}{2}\sum_{n=1}^{\infty}\left\{\frac{|E_n|^2}{4}\left[e^{-cx_I}\left(\frac{e^{2ax_I}}{2a-c}+\frac{e^{-2ax_I}}{-2a-c}-\frac{e^{2ibx_I}}{2ib-c}-\frac{e^{-2ibx_I}}{-2ib-c}\right)-\right.\right.$$

$$\left.\left.-\left(\frac{1}{2a-c}+\frac{1}{-2a-c}-\frac{1}{2ib-c}-\frac{1}{-2ib-c}\right)\right]\right\}.$$

(34) Eastern variance =

$$=\frac{e^{cx_I}}{2}\sum_{n=1}^{\infty}\left\{\frac{|C_n|^2}{4}\left[e^{-cx_F}\left(\frac{e^{-2a(x_I-x_F)}}{2a-c}+\frac{e^{2a(x_I-x_F)}}{-2a-c}-\frac{e^{-2ib(x_I-x_F)}}{2ib-c}-\frac{e^{2ib(x_I-x_F)}}{-2ib-c}\right)-\right.\right.$$

$$\left.\left.-e^{-cx_I}\left(\frac{1}{2a-c}+\frac{1}{-2a-c}-\frac{1}{2ib-c}-\frac{1}{-2ib-c}\right)\right]+\right.$$

$$+\frac{C_n^* D_n}{4}\left[e^{-cx_F}\left(\frac{e^{-2a(x_I-x_F)}}{2a-c}+\frac{e^{2a(x_I-x_F)}}{-2a-c}-\frac{e^{2ib(x_I-x_F)}}{-2ib-c}-\frac{e^{-2ib(x_I-x_F)}}{2ib-c}\right)-\right.$$
$$\left.-e^{-cx_I}\left(\frac{1}{2a-c}+\frac{1}{-2a-c}+\frac{1}{-2ib-c}-\frac{1}{2ib-c}\right)\right]+$$
$$+\frac{C_n D_n^*}{4}\left[e^{-cx_F}\left(\frac{e^{-2a(x_I-x_F)}}{2a-c}+\frac{e^{2a(x_I-x_F)}}{-2a-c}-\frac{e^{-2ib(x_I-x_F)}}{2ib-c}-\frac{e^{2ib(x_I-x_F)}}{-2ib-c}\right)-\right.$$
$$\left.-e^{-cx_I}\left(\frac{1}{2a-c}+\frac{1}{-2a-c}+\frac{1}{2ib-c}-\frac{1}{-2ib-c}\right)\right]+$$
$$+\frac{|D_n|^2}{4}\left[e^{-cx_F}\left(\frac{e^{-2a(x_I-x_F)}}{2a-c}+\frac{e^{2a(x_I-x_F)}}{-2a-c}+\frac{e^{2ib(x_I-x_F)}}{-2ib-c}+\frac{e^{-2ib(x_I-x_F)}}{2ib-c}\right)-\right.$$
$$\left.-e^{-cx_I}\left(\frac{1}{2a-c}+\frac{1}{-2a-c}+\frac{1}{-2ib-c}-\frac{1}{2ib-c}\right)\right]+$$
$$+\frac{|B_n|^2}{4}\left[-e^{-cx_F}\left(\frac{e^{2a(x_F-1)}}{2a-c}+\frac{e^{-2a(x_F-1)}}{-2a-c}-\frac{e^{2ib(x_F-1)}}{2ib-c}-\frac{e^{-2ib(x_F-1)}}{-2ib-c}\right)+\right.$$
$$\left.\left.+e^{-c}\left(\frac{1}{2a-c}+\frac{1}{-2a-c}-\frac{1}{2ib-c}-\frac{1}{-2ib-c}\right)\right]\right\}.$$

Circulation to the east of the barrier

The following expression is used to calculate the contribution to the circulation of the meridional velocity on the eastern side of the barrier. These calculations are shown on all the contour plots and denoted EC. Note that the time dependence has been omitted since the main interest is how this circulation varies for each spatial mode:

$$\text{(35)}\quad \text{EC} = \int_d^{1-d} v_+(x_I)\,dy = \sum_{n=1}^{\infty}\left(-ik\phi_n(x_I)+\frac{\partial\phi_n(x_I)}{\partial x}\right)\frac{\cos(n\pi d)(1-(-1)^n)}{n\pi}.$$

Due to the $(1-(-1)^n)$ term, it is obvious that the modes which are antisymmetric about the mid-latitude and correspond to even Fourier components make a zero contribution to EC.

REFERENCES

PEDLOSKY J., *Geophysical Fluid Dynamics* (Springer, Heidelberg) 1987.

PEDLOSKY J. and SPALL M., *Rossby Normal Modes in Basins with Barriers*, *J. Phys. Ocean.*, **29** (1999) 2332.

PEDLOSKY J., PRATT L. J., SPALL M. A and HELFRICH K. R., *Circulations around islands and ridges*, *J. Mar. Res.*, **55** (1997) 1199-1251.

STOMMEL H. M. and ARONS A. B., *On the abyssal circulation of the world ocean-II. An idealized model of the circulation pattern and amplitude in the ocenanic basins*, *Deep-Sea Res.*, **6** (1960) 217-233.